NUCL SCI TECH (2017) 28:140
DOI 10.1007/s41365-017-0290-z

An energy spectrum smoothing algorithm based on TCC-DEE

Bo Lu[1,2,3] · Yong Chen[1,3] · Yue Zhu[1,3] · Yan-Ji Yang[1] · Wei-Wei Cui[1] · Yu-Mei Zhou[2,3]

Received: 11 November 2016 / Revised: 17 January 2017 / Accepted: 25 January 2017 / Published online: 6 September 2017

Abstract A smoothing algorithm for energy spectrum based on differential nonlinearity (DNL) error elimination with total counts conservation for high-energy particle detector systems is presented. It is physics based and is only determined by the DNL error of analog-to-digital converter device itself. From the experimental results, this algorithm slightly improves both noise performance and energy resolution, while greatly reduces the testing errors by almost a half compared to their original values. In addition, the reduced-χ^2 statistic for evaluating the Gaussian fitting goodness is significantly reduced by almost two orders after smoothing. As a typical verification example, this algorithm is successfully applied in the ground calibration of the Low Energy X-ray Instrument onboard the Hard X-ray Modulation Telescope (HXMT-LE) satellite, lending it a powerful, nondestructive and low-cost tool for both calibration and data processing for high-energy particle detector systems.

Keywords Smoothing algorithm · Energy spectrum · TCC-DEE · DNL error · Low-cost

This work was supported by the HXMT Project and the National Natural Science Foundation of China (No. 11603027).

✉ Bo Lu
luboihep@outlook.com

1 Institute of High Energy Physics, Chinese Academy of Sciences, Beijing 100049, China

2 Institute of Microelectronics, Chinese Academy of Sciences, Beijing 100029, China

3 University of Chinese Academy of Sciences, Beijing 100049, China

1 Introduction

A typical high-energy particle detection system, such as a γ-ray detection system based on cadmium zinc telluride (CdZnTe) [1, 2], a proton detection system using proportional chambers and scintillator counters [3–6] and an X-ray detection system adopting CCDs [7–9], is composed of a detector to convert the particle into electrical signal, an analog front end (AFE) for analog signal processing including linear amplification, shaping, peak holder and discrimination, an ADC to convert the analog signal into digital representation and a digital signal processor (DSP) for control and transmission. In order to alleviate the negative impact of statistical fluctuation nature of such detectors on energy spectrum, a variety of statistics-based smoothing algorithms, including least mean square [13–15], wavelet analysis [10, 11], matched filtering [12] and their combinations and variants, have emerged. However, most of them lack physical basis due to the fact that they alter the total counts after smoothing.

In this paper, we present an energy spectrum smoothing algorithm based on TCC-DEE. This algorithm is only determined by the DNL errors of ADCs, and the negative effect of the electronic systems (without the ADCs) is eliminated through exhaustive contrast experiments. In order to well describe the principle and validity of the algorithm, data from the HXMT-LE [16, 17], a CCD-based soft X-ray detection systems, are used. Although it is based on an X-ray CCD detection system with a specific DNL error, the algorithm can be extended to applications in other high-energy particle detection systems as mentioned previously.

2 DNL error induced problem

The energy spectra obtained by the X-ray CCD detection systems, especially those with large DNL errors, exhibit a common characteristic, regardless of such factors as electronics, X-ray source, pixel rate, temperature, operating time, etc. Figure 1 shows a typical energy spectrum with ^{55}Fe X-ray source, and it is prominent that the count for every fourth counting channel drops, which is smaller than the counts for both of its adjacent channels. This periodic characteristic covers the full-scale output range of the ADC and makes the data points fairly dispersive along the Gaussian fitting curve. Also, thermal vacuum tests adopting the same system confirm that the dropping channels are highly consistent under a wide temperature range from 213 to 313 K.

There are various sources responsible for the DNL errors, among which threshold offset of quantization comparators, periodic spurs dwelling on the power lines, nonlinearity of input signal are three of the most significant sources. Even more complicated, some of them come from the ADC itself, while the rest come from its electronic environment. Fortunately, for purpose of energy spectrum smoothing, it is not necessary to distinguish every source of the DNL error; rather, their combinational effect on the DNL error for every code is sufficient.

3 Smoothing algorithm

In order to eliminate all of the DNL errors, the goal for the smoothing algorithm is to restore the theoretical counts for each code. Based on the energy spectrum problem and electronics principles, the DNL error for every code is the only useful data that can be resorted to. In detail, it has to answer two fundamental questions for the smoothing effect:

1. Is it dependent on the ADC;

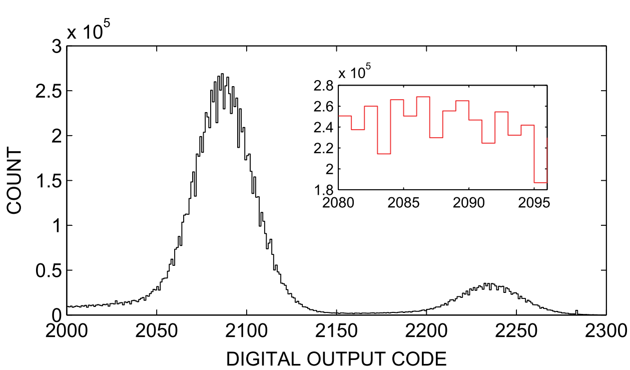

Fig. 1 (Color online) Problem of energy spectrum

2. Is it dependent on the electronic system (without ADC).

The answers will be left to the following sections. In order to avoid ambiguity, the CCD readout system, excluding the ADC device, is called the "electronic system" hereafter. With this convention, investigation of individual effects on energy spectrum of the ADC device and the electronic system is facilitated.

3.1 DNL error and its testing method

Assume n is the output code and N is the resolution of the target ADC, the DNL error is defined as follows [18],

$$\mathrm{DNL}(n) = \frac{V(n) - V(n-1)}{V_{\mathrm{LSB}}} - 1, \quad n \in [1, 2^N - 1], \qquad (1)$$

where $V(n)$ is the corresponding input analog level for the output code, n, and V_{LSB} is the input analog level that a least significant bit (LSB) represents. Therefore, DNL errors of two arbitrary adjacent digital codes are intrinsically relevant by definition, lending DNL(n) a dependent variable from the views of statistics. Fortunately, in the following analysis, an independent-event approximation can be adopted without sacrificing the accuracy.

Since the dominance in testing the DNL error for medium- and high-speed ADC, as the case in HXMT-LE, the sinusoidal code density method (SCDM) [19] is explored in our testing. Taking advantage of DS360 [20] as the high-quality sinusoidal signal generator and well-designed signal-fed strategy, the testing procedure is facilitated and the liability of the output codes is guaranteed.

Assume the theoretical and practical counts for code n in acquiring the DNL error using SCDM are $H_{\mathrm{TS}}(n)$ and $H_{\mathrm{PS}}(n)$, respectively, the corresponding DNL error defined by SCDM is

$$\mathrm{DNL}(n) = \frac{H_{\mathrm{PS}}(n)}{H_{\mathrm{TS}}(n)} - 1. \qquad (2)$$

Under the condition of a large amount of total counts, Eq. (2) makes the DNL(n) an independent variable, which provides a good and reliable approximation to the complicated issue.

As a merit of the target testing method, $H_{\mathrm{TS}}(n)$ can be easily calculated with the help of probability density function of the bathtub curve which is a characteristic of sinusoidal wave. Given the total counts (M_{TS}), and the probability density function of sinusoidal wave for code n ($P_{\mathrm{S}}(n)$), $H_{\mathrm{TS}}(n)$ is expressed as

$$H_{\mathrm{TS}}(n) = P_{\mathrm{S}}(n) M_{\mathrm{TS}}. \qquad (3)$$

From this point of view, $H_{\mathrm{TS}}(n)$ is actually the counts generated by an ideal ADC without DNL errors.

Although DNL errors of most modern ADCs exhibit a mild temperature dependence, the acquisition of DNL errors, as a characteristic of the proposed algorithm, does not require a low-temperature environment as the case where the energy spectrum data (ESdata) are obtained. By contrast, it can be done merely under room temperature, lending this algorithm a good trade-off between the complexity and accuracy.

3.2 Definition of smoothing factors

With the previous analysis, the first-order smoothing factor (SF_1) is defined as

$$SF_1(n) = \frac{1}{DNL(n) + 1}. \tag{4}$$

Therefore, for the target application, the first-order theoretical counts of ESdata ($H_{T1}(n)$) can be directly calculated as the multiplication of $SF_1(n)$ and the practical counts of ESdata ($H_P(n)$).

As an important constraint for the smoothing factor, according to the physical principle, the total counts before and after smoothing should be conservative. However, due to the non-idealities in obtaining DNL(n), SF_1 fails to satisfy the total counts conservation condition. Nevertheless, the resulting maximum total counts error is only about 0.15%, indicating that SF_1 is, in fact, still a fairly accurate approximation. For satisfying the total counts conservation rule, the total counts conservation factor (TCCF) is defined as

$$TCCF = \frac{\sum H_P(n)}{\sum H_{T1}(n)}. \tag{5}$$

Therefore, the second-order smoothing factor (SF_2) can be defined as

$$\begin{aligned} SF_2(n) &= TCCF \times SF_1(n) \\ &= \frac{\sum H_P(n)}{\sum \frac{H_P(n)}{DNL(n)+1}} SF_1(n). \end{aligned} \tag{6}$$

Since SF_2 is superior to SF_1, particularly in terms of total counts conservation, it is used to represent SF hereafter.

4 Smoothing effect

4.1 Experimental setup

In order to answer the questions raised at the beginning of the previous section, three ADCs and two identical sets of electronic systems are adopted. The CCD readout system, shown in Fig. 2, mainly consists of an AFE circuit, an ADC, a field-programmable gate array (FPGA), and a USB transceiver for communication with a monitor (PC). In order to keep the testing condition in line with the situation where a real CCD is used, the CCD driver circuit is included. Five SFs for ADCs are obtained, as shown in Table 1. In addition, two ESdata with ^{55}Fe X-ray source are also obtained using two ADCs and an arbitrary set of electronic system, listed in Table 2. For simplicity, for both SF and ESdata, the first index number denotes ADC device number, while the second index number denotes electronic system number. In addition, the third index number for ESdata, as shown in Table 3, denotes data number merely.

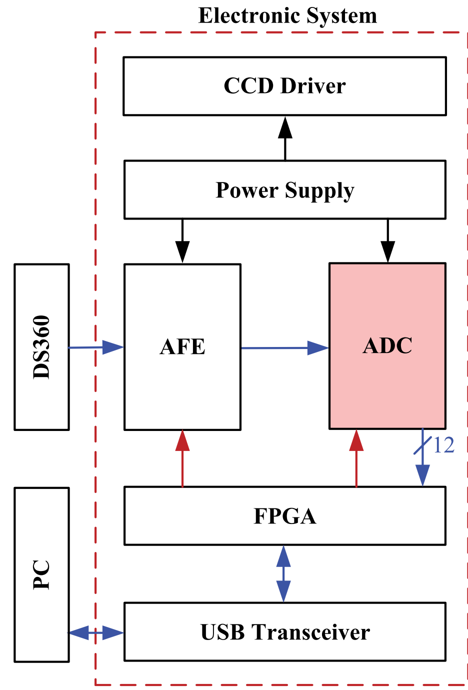

Fig. 2 (Color online) Block diagram of the CCD readout system

4.2 Quantification of smoothing effect

As a powerful tool, Pearson's Chi-squared test (χ^2) [21, 22] is widely used in tests of goodness of fit. In this work, the reduced-χ^2 statistic (χ^2/df) is used, which helps to give a normalized quantitative definition of the

Table 1 Information of SFs

SF	ADC	Electronic system
SF1-1	No.1	No.1
SF2-1	No.2	No.1
SF3-1	No.3	No.1
SF1-2	No.1	No.2
SF2-2	No.2	No.2

Table 2 Information of ESdata

ESdata	ADC	Electronic system
ESdata1-1	No.1	No.1
ESdata2-1	No.2	No.1

smoothing effect of the proposed algorithm. As shown in the following figures, where the abbreviations "BS" and "AS" represent "before smoothing" and "after smoothing," respectively, a successful smoothing is characterized by the fact that χ^2/df for AS is generally smaller than that for BS by almost two orders. One thing deserves mention here, in order to make the figures exhibit the smoothing effect both more explanatory and concise, they are elaborately arranged so that only the main characteristic peak (or K_α line) of ^{55}Fe at 5.9keV is shown.

The smoothing effects using all three SFs from the same No.1 electronic system on ESdata1-1 are shown in Fig. 3. It is clear that SF from an ADC, which is different from the one used to obtain the target ESdata, fails for a successful smoothing. Therefore, the first conclusion can be addressed that the smoothing effect is strongly dependent on the ADC.

The smoothing effects using SFs from No.1 ADC on ESdata1-1 and using SFs from No.2 ADC on ESdata2-1 are shown in Figs. 4 and 5, respectively. It is also clear that SF

Table 3 Noise and FWHM performances comparison

ESdata	Temp./K	Noise_BS/e$^-$	Noise_AS/e$^-$	FWHM_BS/eV	FWHM_AS/eV
ESdata1-1-1	223	13.1 ± 0.3	12.7 ± 0.1	167.9 ± 3.7	167.1 ± 1.7
ESdata1-1-2	218	8.5 ± 0.2	8.2 ± 0.0	150.2 ± 3.6	145.1 ± 1.8
ESdata1-1-3	213	7.3 ± 0.1	7.2 ± 0.0	143.7 ± 3.3	141.6 ± 1.7
ESdata1-1-4	208	6.4 ± 0.1	6.3 ± 0.0	140.8 ± 3.4	139.6 ± 1.8
ESdata1-1-5	203	6.0 ± 0.1	5.9 ± 0.0	138.8 ± 3.3	137.8 ± 1.9

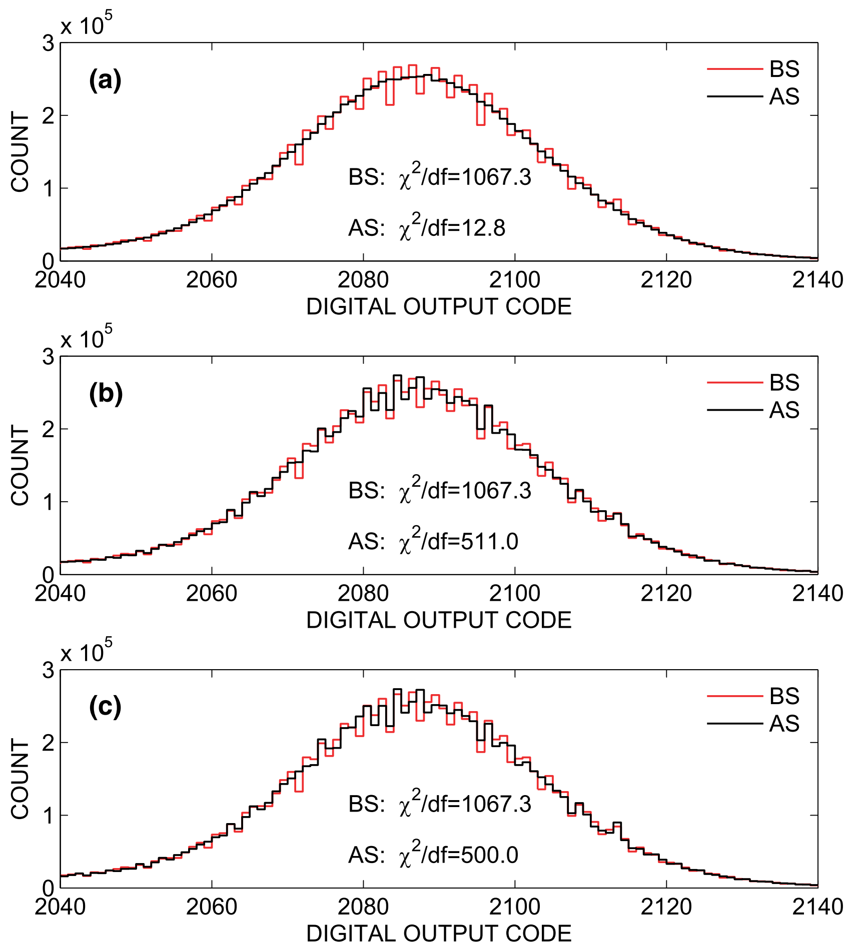

Fig. 3 (Color online) Smoothing effects on ESdata1-1 using **a** SF1-1, **b** SF2-1 and **c** SF3-1

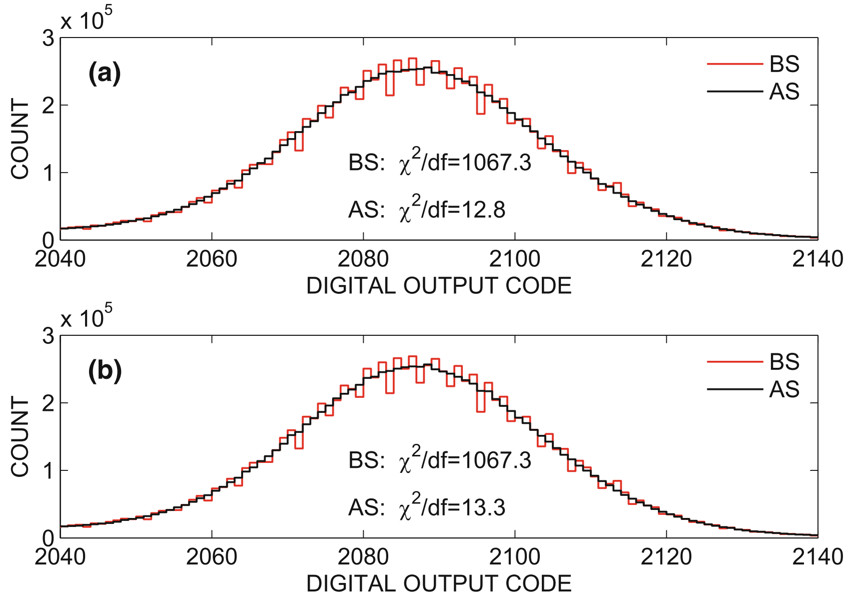

Fig. 4 (Color online) Smoothing effects on ESdata1-1 using **a** SF1-1 and **b** SF1-2

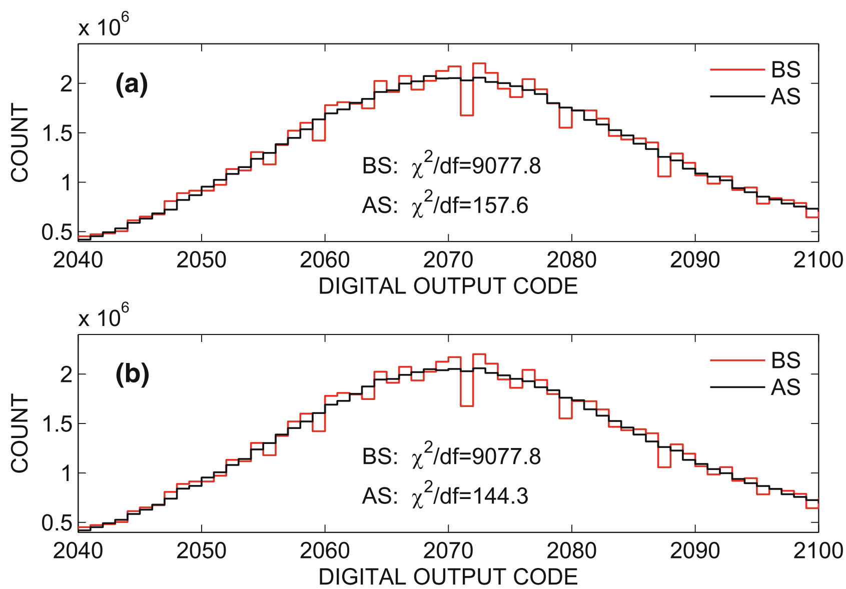

Fig. 5 (Color online) Smoothing effects on ESdata2-1 using **a** SF2-1 and **b** SF2-2

from the same ADC, which is used to obtain ESdata, is competent for a successful smoothing, despite of the difference between the electronic systems for obtaining SF and ESdata. It reaches the second conclusion that the smoothing effect is weakly dependent on the electronic system.

4.3 Efficiency and reliability

In order to verify the efficiency and reliability of the proposed algorithm under conditions with different temperatures and ESdata sizes, the smoothing effects have been investigated over a range of temperature from 203 to 223 K on the ESdata obtained from the combination of No.1 ADC and No.1 electronic system. In addition, the smoothing effects for different data sizes at an arbitrary temperature point, in the vicinity of 213 K in this case, have been compared. The comparison is illustrated in Fig. 6, where χ^2/df for ASs are significantly smaller than that for BSs. It is evident that both variations of temperature and ESdata size hardly have negative influences on the smoothing effect, making it the third conclusion.

However, the proposed algorithm has affected, to a certain extent, the statistical feature of every counting channel, and it is important to investigate the error it introduces. From the mathematical error analysis, as detailed in "Appendix" part, the maximum relative error for a single channel is changed from 16.7×10^{-3} BS to

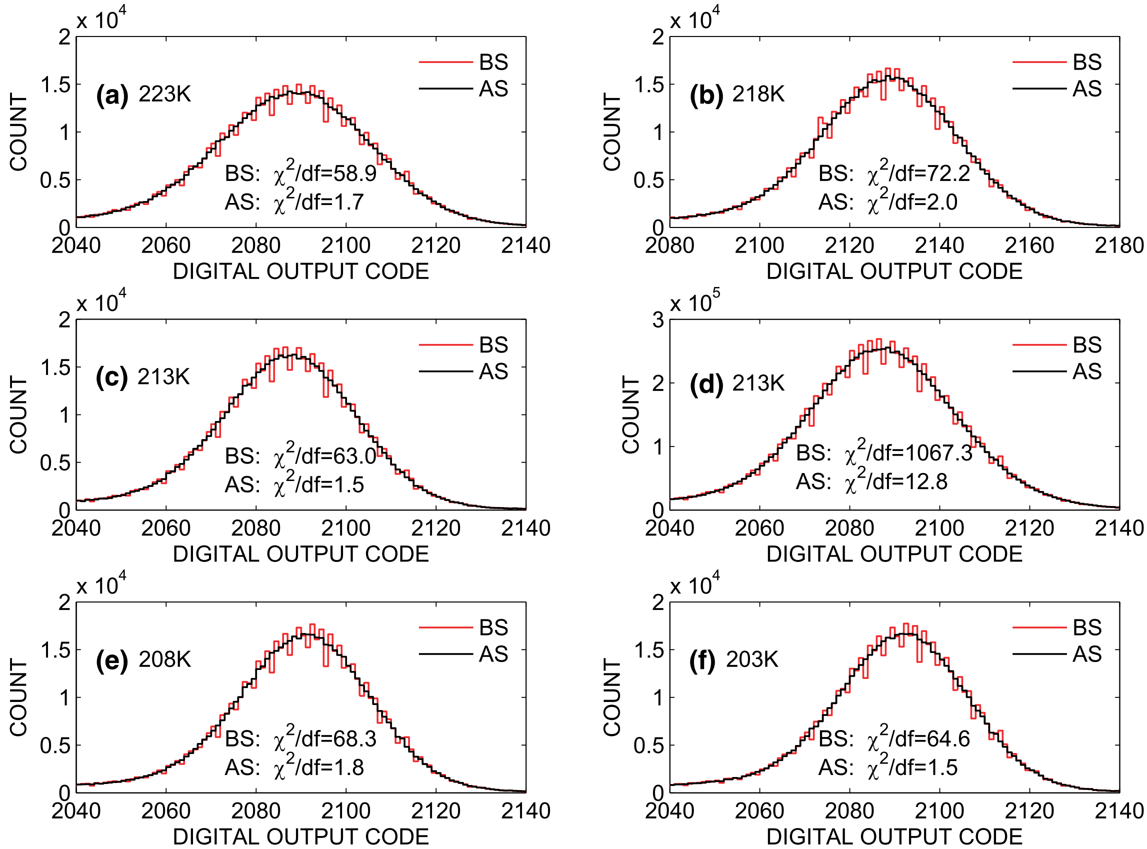

Fig. 6 (Color online) Smoothing effects on different temperatures and ESdata sizes

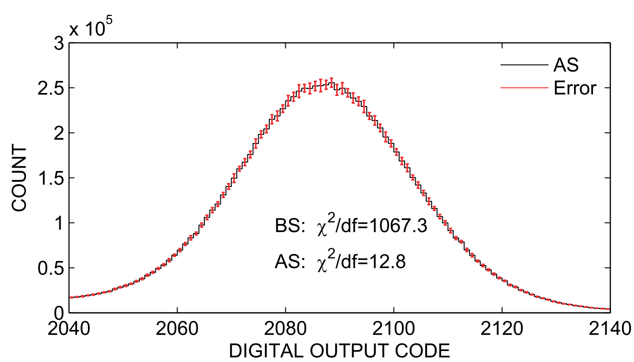

Fig. 7 (Color online) Energy spectrum with error bar

38.7×10^{-3} AS within the range of interest. The AS energy spectrum with error bar is shown in Fig. 7, and it concludes that the error profile is acceptable.

Thus, the proposed smoothing algorithm has good performances on both efficiency and reliability.

4.4 Effect on noise and FWHM

The smoothing effects on the details of the energy spectrum, such as noise and energy resolution defined by full width half magnitude (FWHM), have also been investigated. Using the Gaussian fitting method, the noise and energy resolution can be easily obtained [7, 9]. Table 3 shows some interesting results through five ESdata with almost the same data size as shown in Fig. 6. It confirms that the smoothing algorithm has positive effects on the performance improvement of both noise and energy resolution over a wide temperature range, which is another evidence for the efficiency and reliability of the TCC-DEE algorithm.

5 Discussion and conclusions

Energy spectrum smoothing with TCC-DEE algorithm for the target application is a challenging job, which makes thetrade-off between accuracy and complexity. As a distinguished merit of the proposed smoothing algorithm, SFs are obtained under room temperature. With large amount of total counts, the accuracy can be guaranteed despite the simplicity of the algorithm presented. It has been proved that SFs for the same ADC with different electronic systems are almost consistent with each other and exhibit excellent smoothing effects. It is this important verified conclusion that provides an efficient and reliable way for the calibration of the ADCs used in the flight module of HXMT-LE. More importantly, the presented smoothing algorithm can be further extended to similar applications.

Still, for a more accurate smoothing of energy spectrum with a large DNL error, the following two aspects should be investigated: Firstly, since the reduced count amount of the count-dropping channel is directly distributed between its adjacent channels, it is meaningful to figure out the relationship of the count increments among them; secondly, SF is actually temperature dependent due to the temperature dependent fact of DNL; thus, it makes sense to specify SF for every concerned temperature point. However without a prudential experimental strategy, it will put the flight model ADCs at risk.

As a summary, the presented TCC-DEE smoothing algorithm for energy spectrum is physics based rather than statistics based. It aims to make the analog-to-digital conversion more ideal through the detection and correction of the DNL error. Also, it is hardware oriented rather than data oriented. Although it relies on the data from the instrument to get information of the DNL error, it actually deals with the instrument itself rather than the data that it produces. In addition, it is a nondestructive and low-cost tool for both calibration and data processing for high-energy particle detector systems. The DNL error is corrected by data processing rather than device trimming, greatly reducing the cost.

Appendix

Calculation of χ^2 statistic

Assume the expected count is $H_{\mathrm{E}}(n)$, the χ^2 statistic is calculated as

$$\chi^2 = \sum \frac{\left(H_{\mathrm{P}}(n) - H_{\mathrm{E}}(n)\right)^2}{H_{\mathrm{E}}(n)}. \tag{7}$$

$H_{\mathrm{E}}(n)$ is calculated as follows

$$H_{\mathrm{E}}(n) = P_{\mathrm{G}}(n) \sum H_{\mathrm{P}}(n). \tag{8}$$

where $P_{\mathrm{G}}(n)$ is the probability density function of a Gaussian distribution, which uses an estimated mean and standard deviation from $H_{\mathrm{P}}(n)$. Therefore, the degree of freedom (*df*) is calculated as

$$df(\chi^2) = df(H_{\mathrm{P}}) - 3. \tag{9}$$

Calculation of $\sigma^2(\mathrm{SF}(n)H_{\mathrm{P}}(n))$

Two facts are beneficial to the error analysis. One is that TCCF is a small quantity, and its error is neglected for simplicity. The other is that $H_{\mathrm{P}}(n)$ is irrelevant to $H_{\mathrm{PS}}(n)$. Therefore, according to the error transfer principle, $\sigma^2(\mathrm{SF}(n) \times H_{\mathrm{P}}(n))$ can be derived. Note that for simplicity, quantities in vector forms as previously used are now reduced to simple symbols; for example, $H_{\mathrm{P}}(n)$ is replaced by H_{P}.

The expression of counts after smoothing is

$$\mathrm{SF} \times H_{\mathrm{P}} = \frac{H_{\mathrm{P}}}{H_{\mathrm{PS}}} P_{\mathrm{S}} \sum H_{\mathrm{PS}}. \tag{10}$$

From the previous analysis, the complete expression of $\sigma^2(\mathrm{SF} \times H_{\mathrm{P}})$ is

$$\begin{aligned}\sigma^2(\mathrm{SF} \times H_{\mathrm{P}}) = {} & \left(\frac{1}{H_{\mathrm{PS}}}\right)^2 \sigma^2(H_{\mathrm{P}}) \\ & + \left(\frac{H_{\mathrm{P}} P_{\mathrm{S}} \sum H_{\mathrm{PS}}}{H_{\mathrm{PS}}}\right)^2 \sigma^2(H_{\mathrm{PS}}) \\ & + \left(\frac{H_{\mathrm{P}} P_{\mathrm{S}}}{H_{\mathrm{PS}}}\right)^2 \sum \sigma^2(H_{\mathrm{PS}}).\end{aligned} \tag{11}$$

Due to the fact that H_{P} and H_{PS} follow Poisson distributions, their deviations are expressed as

$$\sigma^2(H_{\mathrm{P}}) = H_{\mathrm{P}}, \tag{12}$$

$$\sigma^2(H_{\mathrm{PS}}) = H_{\mathrm{PS}}. \tag{13}$$

Definition of relative error

The relative error ($\mathrm{RE}(n)$) for each counting channel is defined as the ratio of error to count

$$\mathrm{RE}(n) = \frac{\sigma(H_{\mathrm{P}}(n))}{H_{\mathrm{P}}(n)}. \tag{14}$$

References

1. M. Prokesch, S.A. Soldner, A.G. Sundaram et al., CdZnTe detectors operating at X-ray fluxes of 100 million photons/(mm^2 sec). IEEE Trans. Nucl. Sci. **63**, 1854–1859 (2016). doi:10.1109/TNS.2016.2556318
2. P. Xu, S. Wang, X.H. Cai et al., The extraction and smoothing algorithms for gamma-ray spectrum of a CdZnTe detector system. Nucl. Sci. Tech. **25**, 50402–050402 (2014). doi:10.13538/j.1001-8042/nst.25.050402
3. G.F. Hartner, D.E. Blodgett, S.B. Bracker et al., A recoil proton detector using cylindrical proportional chambers and scintillator counters. Nucl. Instrum. Methods **216**, 113–119 (1983). doi:10.1016/0167-5087(83)90337-X
4. G.D. Alkhazov, A.A. Vorobyov, A.V. Dobrovolsky et al., Investigation of the structure of light exotic nuclei by proton elastic scattering in inverse kinematics. Phys. Atom. Nuclei **78**, 381–386 (2015). doi:10.1134/S1063778815020076
5. T.L. Collums, M.R. Islam, E.R. Benton et al., Comparison of plastics used in proportional counters for proton and heavy ion

measurements. Nucl. Instrum. Methods B **333**, 69–72 (2014). doi:10.1016/j.nimb.2014.04.016
6. Z. Fu, Y. Heng, S. Gu et al., Efficiency-determined method for thermal neutron detection with inorganic scintillator. Nucl. Sci. Tech. **24**, 40205–040205 (2013). doi:10.13538/j.1001-8042/nst.2013.04.010
7. B. Lu, W.W. Cui, Y.S. Wang et al., Design and optimization of the readout system for X-ray CCDs. Chin. Phys. C **36**, 846–855 (2012). doi:10.1088/1674-1137/36/9/009
8. B. Lu, Y.S. Wang, Y. Chen et al., Hard X-ray imaging techniques based on CCD and CsI Scintillator. Optic. Precis. Eng. (2012) **(in press)**
9. Y.C. Wang, X.F. Cao, Q. Yu et al., A fully integrated 0.055% INL X-ray CCD readout ASIC with incremental ΔΣADC. IEEE Tran. Nucl. Sci **63**, 1733–1739 (2016). doi:10.1109/TNS.2016.2543261
10. P. Bury, N. Ennode, J.M. Petit et al., Wavelet analysis of X-ray spectroscopic data part I. The method. Nucl. A **383**, 572–588 (1996). doi:10.1016/S0168-9002(96)00721-8
11. G. Xiao, L. Deng, B. Zhang et al., A nonlinear wavelet method for data smoothing of low-level gamma-ray spectra. J. Nucl. Sci. Technol. **41**, 73–76 (2004). doi:10.1080/18811248.2004.9715460
12. M. Gu, L.Q. Ge, Smoothing technology of gamma-ray spectrometry data based on matched filtering. Nucl. Electron. Detect. Technol. **29**, 978–980 (2009). doi:10.3969/j.issn.0258-0934.2009.05.012
13. P.A. Gorry, General least-squares smoothing and differentiation by the convolution (Savitzky–Golay) method. Anal. Chem. **62**, 570–573 (1990). doi:10.1021/ac00205a007
14. H. Lu, X. Li, T. Hsia et al., Analytical noise treatment for low-dose CT projection data by penalized weighted least-square smoothing in the KL domain. Proc. SPIE **4682**, 146–152 (2002). doi:10.1117/12.465552
15. D. Alberto, E. Falletti, L. Ferrero et al., FPGA implementation of digital filters for nuclear detectors. Nucl. Instrum. Methods A **611**, 99–104 (2009). doi:10.1016/j.nima.2009.09.049
16. F.J. Lu, The current status of the hard X-ray modulation telescope. Proc. SPIE **5900**, 266–275 (2005). doi:10.1117/12.925620
17. Y.S. Wang, Y. Chen, Y.P. Xu et al., Low temperature testing and neutron irradiation of a swept charge device on board the HXMT satellite. Chin. Phys. C **36**, 991–995 (2012). doi:10.1088/1674-1137/36/10/013
18. IEEE Standard for Terminology and Test Methods for Analog-to-Digital Converters, IEEE Standard 1241–2010, 2011, 46–64. doi:10.1109/IEEESTD.2011.5692956
19. W. Kester, *The Data Conversion Handbook* (Newnes, Burlington, 2005), pp. 303–316
20. DS360-Ultra-low distortion function generator, Datasheet. Stanford Research Systems.http://www.thinksrs.com/downloads/PDFs/Catalog/DS360c.pdf
21. A. DasGupta, *Asymptotic Theory of Statistics and Probability* (Springer, New York, 2008), pp. 441–450
22. Y.S. Zhu, *Probability and Statistics in Experimental Physics* (Science Press, Beijing, 2006), pp. 410–425